Thermal Analysis and Crystallization of $M_Y(Sb_{70}Te_{30})_{100-Y}$ (M = Ag, Sn; Y = 0, 7.5) Amorphous Thin Films

Javier Rocca
Universidad de Buenos Aires - CONICET https://orcid.org/0000-0002-4233-2949
María Andrea Ureña
Universidad de Buenos Aires - CONICET https://orcid.org/0000-0001-8900-5243
Marcelo Fontana (mfontan@fi.uba.ar)
Universidad de Buenos Aires - CONICET https://orcid.org/0000-0002-4861-0997

Research Article

Keywords: Phase-change materials, Crystallization of antimony-telluride thin films, Differential scanning calorimetry, Transformation diagrams

Posted Date: December 28th, 2023

DOI: https://doi.org/10.21203/rs.3.rs-3808188/v1

Additional Declarations: The authors declare no competing interests.

Abstract

Antimony-telluride based phase-change materials doped with different metals have been proposed to be ideal materials for improving the performance of phase-change memories. It is well known that Sb70Te30 thin films show a sharp fall in the electrical resistance in a narrow temperature range when heating. Therefore, it is interesting to study the effect of adding metallic atoms into this composition. In this work, the crystallization of My(Sb0.70Te0.30)100-y (M = Ag, Sn; y = 0, 7.5) amorphous thin films, obtained by pulsed laser deposition, has been studied by means of differential scanning calorimetry under continuous heating regime. The as-deposited samples and the crystallization products have been characterized by X-ray diffraction. The crystallization and melting temperatures were determined, as well as the enthalpies involved in such processes. The activation energy for crystallization was also determined. From the obtained results, it is observed that the addition of metals shifts the crystallization process to higher temperatures around 15-25 K and increases its activation energy. The transformation diagrams (Temperature-Time-Transformation and Temperature-Heating rate-Transformation) are calculated. The experimental results are discussed and correlated with proposed structures for the glass and the crystalline states. The present results are also compared with those reported by other authors.

1. Introduction

The use of chalcogenide phase change materials (PCM) [1–6] holds great promise for memories new design in response to the increasing demand for data storage and processing, driven by artificial intelligence and other applications with data intensive use. Phase change memories take advantage of the fast and reversible phase transitions between the amorphous and crystalline states for switching, where crystallization and amorphization are the processes that allow changing the logical state of the PCM memory. The change in electrical resistance between the amorphous (high resistance) and crystalline (low resistance) states is used to identify the logical states ("0" and "1") of memories [1–6]. PCM, that are frequently obtained as thin films, are grouped in different families, being the alloys of the Ge-Sb-Te system one of most studied chalcogenide glasses. In a previous work, the structural and electrical behaviors with the temperature of thin films with compositions $Ge_{13}Sb_5Te_{82}$, $Ge_1Sb_2Te_4$, $Ge_2Sb_2Te_5$, $Ge_1Sb_4Te_7$ and $Sb_{70}Te_{30}$ were studied [7]. The electrical resistance contrast in these alloys is between 3 and 6 orders of magnitude and it is feasible to generate multiple intermediate resistance states by tuning the amorphous-crystalline ratio in a single memory cell [7, 8].

Some of the most outstanding systems for PCM are $(Sb_2Te3)_m(Sb_2)_n$ structures consisting of Sb_2-and Sb_2Te_3-type slabs stacked along [001] direction. Depending on the total number of slabs (and relative to each other), structures with $P\bar{3}m$ (Sb_2Te, SbTe) or $R\bar{3}m$ (Sb_2Te_3, Sb_8Te_3, Sb_4Te_3) space group are usually formed [9, 10]. In the Sb-Te system, the Sb-rich alloys of composition close to $Sb_{70}Te_{30}$ stands out for their good properties.

1.1 Alloys based on $Sb_{70}Te_{30}$

One of the most suitable materials for non-volatile storage is the $Sb_{70}Te_{30}$ composition [1]. With the aim of improving the performance of PCM-based memories, the effect of adding an impurity such as Al, Ag, In, Ge, Mg or Zn in $Sb_{70}Te_{30}$ glasses has been studied, observing an improvement in properties like crystallization temperature, activation energy and crystallization rate [11–19]. This fact is corroborated in the same Sb-Te binary system, where a dopant element (Cr, Ru, Cu, Si, Zr, Ti or W) is added to improve the performance in phase memories of another alloy rich in Sb and close in composition: $Sb_{67}Te_{33}$. [20–26].

On the other hand, in a previous work, using Rietveld refinements of the experimental XRD patterns and ab-initio calculations, when studying powder crystalline samples $Sn_x[Sb_{0.70}Te_{0.30}]_{100-x}$, (with x = 0.0, 2.5, 5.0 and 7.5 at. %), we showed [27] that the increase of tin content in the $Sb_{70}Te_{30}$ compound lead to the progressive distortion of the crystalline structure, favoring a second-order transition from the reference trigonal structure (space group P_{-3m1}) to a monoclinic structure (space group $C_{2/m}$). The gradual doping of the $Sb_{70}Te_{30}$ alloy with Sn causes a soft shift of the positions of some peaks in the X-ray diffractograms [27] as a result of a very slight structure distortion (the angle β of this structure changes from 90.00 to 90.14). Ab initio calculations show Sn atoms substitute Sb atoms in the Sb-Te host in an octahedral environment with similar bond lengths to those of $Sb_{70}Te_{30}$. From now on this crystalline phase is called δ − phase.

In this work, $M_y(Sb_{0.70}Te_{0.30})_{100-y}$ (M = Ag, Sn; y = 0, 7.5) amorphous thin films obtained by pulsed laser deposition are analyzed. Our goal is to study the influence of tin and silver addition to $Sb_{70}Te_{30}$ glass in crystallization and melting processes. The knowledge of the mechanisms affecting the transformation kinetics is the base of microstructural control to optimize physical properties of chalcogenide glasses. Differential scanning calorimetry (DSC) has been used for the determination of both the thermal stability of the glassy alloys and the apparent activation energy of crystallization. The main mechanisms that drive the crystallization process of the ternary glasses are analyzed and compared with those acting on the binary eutectic. The results are correlated with the structures proposed for the glass and the crystalline states. The transformation diagrams (Temperature-Time-Transformation and Temperature-Heating rate-Transformation) are calculated.

2. Experimental

$M_y(Sb_{0.70}Te_{0.30})_{100-y}$ (M = Ag, Sn; y = 0, 7.5 at. %) thin films were prepared by pulsed laser deposition (PLD) from bulk chalcogenide targets. Bulk targets were prepared by direct synthesis loading 10 mm diameter quartz tubes with pure elements (4N) in their stoichiometric proportions. Loaded tubes were evacuated and sealed at $3 \cdot 10^{-5}$ mbar, and then heated at 800°C for 8 h. Melts were slowly cooled down to room temperature inside the furnace. Bulk samples were sliced and polished in order to obtain PLD targets with parallel faces. The studied compositions are named as indicated in Table 1.

PLD was performed using a nanosecond-pulsed Nd:YAG laser (Spectra-Physics Quanta-Ray Lab-150) with deposition times of 45–60 minutes, operating at a 355 nm wavelength. Thin films were deposited on

chemically cleaned microscope glass slides in on-axis geometry at room temperature inside vacuum chamber [7, 28].

Thermal analysis was carried out in a Perkin Elmer Pyris 1 differential scanning calorimeter (DSC) in the temperature range from 300 K to 600 K under a continuous heating regime at scan rates β = 10, 20, 40 and 80 K/min. In order to observe the melting process, an annealing per sample was carried up to 873 K. The experiments were done in a dynamic Ar atmosphere using sealed aluminium pans containing deposited films that were mechanically extracted from glass substrates. Mass of samples was weighted between 2.00 and 4.50 mg, with a precision of 10 µg.

X-Ray Diffraction experiments were done with monochromatized Cu-Kα radiation on a Smartlab Rigaku diffractometer., As-deposited films were measured in grazing incidence geometry with a grazing angle ω = 0.5°, sweeping at 0.16º/min with 0.05º steps. Thermally treated films were measured in Bragg-Brentano geometry, sweeping at 0.2º/min with 0.05º steps.

3. Results

Figure 1 shows the calorimetric signal (normalized by the mass and the heating rate) dH/dT of the samples obtained under a continuous heating regime with β = 40 K/min. Calorimetric curves show one or more exothermic transformations, depending on the composition of samples. The $Sb_{70}Te_{30}$ binary sample has a single symmetric peak that could be associated with a single process. Ternary samples, on the other hand, exhibit more complex situations. In the AST7.5 sample there are three superimposed exothermic transformations which are resolved by observing their respective peak temperatures, while in the SST7.5 sample there is an asymmetric peak, which may indicate the existence of a complex crystallization involving more than one process. This fact is confirmed when sweeps at different speeds are carried out, as can be seen in Fig. 2. At low speeds, at least two superimposed processes associated with the main exothermic peak are clearly observed, which are not resolved at higher speeds.

X-ray diffractograms of both as-deposited and thermally treated films are displayed in Fig. 3 (a). X-ray patterns of the PLD as-obtained films are characteristic of an amorphous phase with a minoritary crystalline phase. Figure 3 (a) shows a broad scattering peak associated to amorphous phase that does not depend on the concentration and is located at $Q = 4\,\pi.\,\sin(\theta)/\lambda = (2.06 \pm 0.02)$ Å^{-1} in agreement with previous works [7, 29] and close to the values of Sb liquid (Q = 2.15 Å^{-1} at T = 933 K) and Te liquid (Q = 2.10 Å^{-1} at T = 743 K) [30]. After DSC thermal treatments, films become crystalline as it can be appreciated from the shown patterns.

X-ray data of $Sb_{70}Te_{30}$ and SST7.5 powder samples associated to trigonal structure ($P_{\bar{3}m1}$ space group) and monoclinic structure ($C_{2/m}$ space group) respectively are shown in Fig. 3 (b) for comparison purposes. This figure shows that both structures have few differences in their pattern diffractograms. Actually, δ-phase has a continuous second order transition from $P_{\bar{3}m1}$ to $C_{2/m}$ when a third element is added to the composition $Sb_{70}Te_{30}$.

The three crystalline peaks of the as-deposited and thermally treated films observed in $Sb_{70}Te_{30}$, SST7.5 and AST7.5 diffractograms (see Fig. 3 (a)) correspond to the crystalline lines of both previously reported crystalline structures (trigonal P_{-3m1} and monoclinic $C_{2/m}$ structures) that are associated with similar crystalline structures corresponding to δ-phase.

On the other hand, a broadening of the crystalline peaks, associated with a nanometer-scale grain size, is observed in Fig. 3 in both as-deposited and thermally treated films.

Figure 4 shows DSC curves of $Sb_{70}Te_{30}$ samples for all heating rates. The observed behavior when changing heating rates is representative of a single transformation process and we see that the peak maintains its shape for all treated rates. Changes in the crystallization peak temperature T_p of the binary sample determined for different values of β are presented in Table 2. Crystallization temperature T_p at 10 K/min is in accordance with value reported by Her et al [31] when measuring film reflectivity variation upon heating at same rate.

Cristallization peak temperatures of ternary samples, as well as onset T_{on} and melting T_m temperatures, crystallization ΔH_c and melting ΔH_m enthalpies, of all samples are also shown in Table 2. An important result is that the addition of Sn or Ag to the binary composition shifts the crystallization process to higher temperatures around 15–25 K. Values of T_{on}/T_m ratio (crystallization temperature to melt temperature ratio) are between 0.49 and 0.55. This is a good property for applications in PCM-based memories. We notice that onset and peak temperatures increase with tin or silver content. Similar behaviors are reported when a third element (Al, Ag, Cr, Cu, Ga, Ge, In, Mg, Ru, Si, Ti, W, Zn, Zr) is added to $Sb_{67+y}Te_{33-y}$ ($0 \leq y \leq 13$) [11–26, 33–36]. In particular, Hsu et al [13] found that crystallization temperatures for $Sb_{69.9}Te_{30.1}$, $Ag_4(Sb_{70}Te_{30})_{96}$ and $Ag_{10.8}(Sb_{70}Te_{30})_{89.2}$ are 409 K, 413 K and 427 K respectively, in good agreement with this work.

As seen in Figs. 3 and 4, as β increases, transformations shift to higher temperatures, showing a thermally activated nature of the process. The activation energy E_a can be determined by the Kissinger method [37]:

$$ln\left(\frac{\beta}{T_p^2}\right) = \frac{E_a}{RT_p} + c$$

1

where R is the universal gas constant, T_p is the temperature at which the minimum of the crystallization peak is reached and c is a constant.

Therefore, E_a is obtained from the slope of the linear fit in $ln\left(\frac{\beta}{T_p^2}\right)$ versus $1000/T_p$ graph. Figure 5 shows these graphs for the main peak of each studied sample. The results obtained from the activation

energy are shown in Table 2. The addition of a third element to the binary composition produces an increase in the value of the activation energy for crystallization. This fact was widely observed in other cases [11–26, 33–36]. In particular, Hsu et al [13] found that the activation energies for the crystallization of $Sb_{69.9}Te_{30.1}$, $Ag_4(Sb_{70}Te_{30})_{96}$ and $Ag_{10.8}(Sb_{70}Te_{30})_{89.2}$ are 200,7 kJ/mol, 220,1 kJ/mol and 251,8 kJ/mol respectively in good agreement with this work.

The range for the T_p/T_m ratio is between 0.51 and 0. 55, while Hsu et al reported T_p/T_m = 0.6 (both results with 10 K/min heatings) [13].

4. Discussion

The fact that the observed transformation for the binary sample is due to a single process allows a deeper analysis of the crystallization kinetics. The temperature dependence of the transformation rate dx/dt can be determined for each heating rate and the transformed fraction x from the following relation [38, 39]:

$$x(T) = \frac{\Delta H(T)}{\Delta H_{crist}} = \frac{\int_{T_o}^{T} \frac{dH}{dT} dT}{\int_{T_o}^{T_e} \frac{dH}{dT} dT}$$

2

where $\Delta H(T)$ is the partial area from T_o to temperature T of the calorimetric signal normalized by the mass and the heating rate, T_o and T_e are the start and end temperatures of the peak. Figure 6 shows x and the transformation rate dx/dt normalized by the heating rate (that is dx/dT) for the crystallization of the binary sample as a function of the heating rate β.

In the case of ternary compositions, understanding the transformation kinetics is more difficult because the DSC signal is associated with two or more superimposed processes. This implies that in order to carry out an adequate processing, additional methodologies of an experimental nature must be followed with the addition of numerical simulations that allow separating each of the processes. This is impossible to do with the obtained experimental information. However, it can be assumed that the first steps of the transformation recorded by calorimetry are due to a single first process and that the overlap with other processes occurs later [38, 39].

On the other hand, it was found that $Sb_{67}Te_{33}$ and other Sb-rich alloys have faster reversible phase change character owing to its growth-dominant mechanism with negligible nucleation [18, 40–42]. Therefore, it can be expected that the crystallization is controlled by grain growth without nucleation for the studied samples in this work. Moreover, in a previous work [43] we found that three-dimensional growth of pre-existing nuclei is the governing mechanism in the crystallization of $Sb_{70}Te_{30}$ binary thin films. Due to the structural information obtained by X-rays and the closeness in their compositions, we

assume the same mechanism for ternary samples. Under this hypothesis, we are able to model first crystallization steps for the three studied compositions and construct the transformation diagrams.

4.1 Initial steps of crystallization

Following previous works [44–47], the initial steps of the formation of crystals (crystalline fraction $x < 0.1$) are modeled from experimental calorimetric data. The crystallization of these glasses is complex. However, as mentioned above, the first steps of the crystallization of the samples can be modeled assuming three-dimensional interface-controlled crystal growth of pre-existing nuclei with mean density N_v [48].

The classical equations used for the growth rate u are expressed as [46, 49, 50]:

$$u\left(T\right) = \left(a_o \lambda b/\eta\right)[1 - exp(-\Delta G/RT\ )]$$

3

$$b = kT/\left(3\pi L^2 a_o^3\right)$$

where a_o is the mean atomic diameter, T is the temperature, λ is the product of the fraction of surface sites where atoms are preferentially added and the length of the interface in units of a_o, L is the mean interfacial thickness in units of a_o, and η is the viscosity. The dependence of η with T follows a Vogel-Fulcher expression [20–21]:

$$\eta = \eta_o exp(A/(T - To\ ))$$

4

In (3) ΔG is the Gibbs free-energy difference between the supercooled liquid and the crystal [49, 50]:

$$\Delta G = \Delta H_m\ [(\ 1 - T_r\ )(\ 1 - \Gamma) - \Gamma T_r ln(T_r\ )]$$

5

Here $T_r = T/T_m$, $\Gamma = \Delta C_p/\Delta S_m$, ΔC_p is the heat capacity difference between the liquid and the crystal, T_m, ΔS_m and ΔH_m are the melting temperature, melting entropy and melting enthalpy, respectively.

For a process of three-dimensional interface-controlled crystal growth of pre-existing nuclei, the time temperature transformation (TTT) and temperature-heating rate-transformation (THRT) diagrams can be calculated using [44–46, 51, 52]:

$$\backslash \mathrm{varvec}x(T,t) = 1 - exp(-(4\pi/3).N_v.u\left(T\right)^3.t^3)$$

6

[TTT diagrams – pre-existing nuclei and growth]

with t the time,

$$\varvec{x}(T,\beta) = 1 - exp(-(4\pi/3)N_v[\int_{T_0}^{T} u\left(T'\right) dT'/\beta]^3)$$

7

[THRT diagrams – pre-existing nuclei and growth]

with β the heating rate.

4.2 Initial steps of crystallization for the $Sb_{70}Te_{30}$, AST7.5 and SST7.5samples

As mentioned above, we assume that δ-phase crystallizes in the $Sb_{70}Te_{30}$, AST7.5 and SST7.5 samples.

The first steps of crystallization for these samples were modeled assuming the three-dimensional interface-controlled crystal growth of pre-existing nuclei. We calculated the TTT and THRT curves using calorimetric data obtained under continuous heating rate regimes using Eq. (3) to (7). In these equations we assumed that parameters that were not measured in our experiments (a_o, ΔC_p, L^2/λ, and $\eta(T_m)$) are the same in all the samples and they were determined as following: a_o was estimated using a weighted average of the atomic radii of the elements; ΔC_p = 0.15 J/g K was estimated using data for Te and Se based glasses [53]; L^2/λ = 1 was estimated using the work of Clavaguera-Mora et al. [46]; $\eta(T_m)$ was estimated using the values of viscosity at melting point for PCM chalcogenide glasses [54–55]. ΔH_m and T_m were measured for each sample in DSC experiments, so ΔS_m and Γ were calculated as $\Delta H_m/T_m$ and $\Delta C_p/\Delta S_m$ respectively. N_v/L^2, A and T_o were fitted using Eqs. (6) and (7) to reproduce the experimental DSC data (x = 0.1) in all the samples. Measured, estimated as well as fitted parameters are given in Table 3.

Calculated temperature-heating rate (THrT) and time temperature transformation (TTT) curves for different crystallized fractions (x = 10^{-6}, 10^{-3} and 0.1) as well as experimental data obtained for x = 0.1 are reported in Figs. 7 and 8. We observe a very good agreement between the calculated curve and the experimental data.

The glass temperature T_g can be determined assuming that the viscosity at the glass temperature $\eta(T_g)$ is about 10^{12} Pa·s. Obtained values of T_g for *$Sb_{70}Te_{30}$*, *AST7.5* and *SST7.5 samples* are 357.5 K, 381.5 K and 378 K respectively. The addition of Ag or Sn increases the glass temperature. This fact was also observed when Ag or Sn was added to Sb_2Te binary composition (near *$Sb_{70}Te_{30}$*) [56]. Prokhorov et al [33] found the expression $T_g = x_{Sb}$ 420 K + x_{Te} 204 K (with x_{Sb} and x_{Te} the atomic fraction of Sb and Te

respectively to determine T_g in Sb-Te binary alloys). When evaluating this expression for $Sb_{70}Te_{30}$, a value of 355 K is obtained. This is in good agreement with our estimation from η(T_g).

The transformation diagrams shown in Figs. 7 and 8 are essentially built from experimental DSC measurements, where the limiting mechanism is the mobility of atoms, which is characterized by the viscosity. The viscosity, shown in Fig. 9 for the three samples, follows Eq. (4), where its parameters are obtained from fitting of transformation diagrams. In this figure, we highlight the temperature ranges corresponding to glass transition, crystallization and melting. The addition of a third element to the binary composition $Sb_{70}Te_{30}$ increases the viscosity, as well as the glass temperature, T_g/T_m and T_{on}/T_m.

4.3 Structure and PCM switching

The structures of liquid and amorphous $Sb_{67}Te_{33}$ phases were studied by Kang et al [57]. In amorphous $Sb_{67}Te_{33}$, Sb and Te atoms are almost in an octahedral environment, as occurs in crystalline phase. They suggest that structural similarity of octahedrons between the crystalline and amorphous phases promotes the rapid and low-energy switching of $Sb_{67}Te_{33}$.

In this work, the crystallization of $M_y(Sb_{70}Te_{30})_{100-y}$ (M = Ag, Sn; y = 0, 7.5) amorphous thin films, obtained by pulsed laser deposition, have been studied by means of differential scanning calorimetry under continuous heating regime. Considering that:

1. It is expected that the amorphous structure of the three studied samples is the same as that of the $Sb_{67}Te_{33}$ composition glass, due to the closeness in composition. This means that both Sb and Te atoms are almost in an octahedral environment.
2. X-ray patters of crystallized samples in this work are similar for the three samples. Their crystalline structures correspond to trigonal structure (space group P_{-3m1}) for the $Sb_{70}Te_{30}$ binary sample and is a very slight distortion to monoclinic structure (space group $C_{2/m}$) with the addition of Sn. This distortion can be seen in the variation of the β angle of the structure (changes from 90.00 to 90.14). It is important to highlight that these structures have a predominance of octahedral environments. Moreover, the crystalline structure of $Sb_{67}Te_{33}$ is the same crystalline structure
3. In the case of *SST7.5*, we found in a previous work, that Sn atoms in the monoclinic crystalline structure substitute Sb atoms and are in an octahedral environment with six coordination of Te atoms. Moreover, considering that Sn-Te bond (338,1 KJ/mol in [58]) has greater dissociation energy than Sb-Te bond (277,4 KJ/mol in [58]), the crystallization temperature in *SST7.5* is expected to be higher than in the $Sb_{70}Te_{30}$ binary sample. This agrees with crystallization temperatures that are reported in this work.

Therefore, it can be concluded that the ideas of Kang et al [57] can be used for the studied samples in this work. The key for understanding rapid glass-crystal transition in the studied samples for their application in PCM memories is the structural similarity of octahedrons between crystalline and amorphous phases.

5. Conclusions

In this work, the thermal evolution of thin films obtained by PLD of compositions $M_y (Sb_{70}Te_{30})_{100-y}$ (M = Sn, Ag; y = 0, 7.5) was analyzed and compared with the binary $Sb_{70}Te_{30}$. The addition of a third metallic element, Ag or Sn, generates a delay in the crystallization temperature and an increase in the activation energy for crystallization. This fact implies that the amorphous state is more stable, and therefore it improves the properties for applications in non-volatile memories, since it broadens its thermal range. The crystallization of the binary sample could be associated to a single process, whereas the crystallization of the ternary samples is more complex. The parameter T_{on}/T_m of the studied films show good values for the application in non-volatile memories.

The TTT and THrT transformation diagrams were calculated for the first stages of crystallization, which allows us to predict how these alloys will behave for other thermal evolutions different from those carried out in this work.

Declarations

Authorship Contribution

All authors contributed to the study conception and design. Material preparation, data collection were performed by María Andrea Ureña and Javier Rocca. Analysis were performed by Marcelo Fontana, Javier Rocca and María Andrea Ureña. The first draft of the manuscript was written by Marcelo Fontana and all authors commented on previous versions of the manuscript. All authors read and approved the final manuscript.

Acknowledgments

This work has been partially supported by Universidad de Buenos Aires, Agencia Nacional de Promoción de la Investigación, el Desarrollo Tecnológico y la Innovación (Argentina) and Consejo Nacional de Investigaciones Científicas y Técnicas - CONICET (Argentina).

References

1. Wuttig, M., Yamada, N. Phase-change materials for rewriteable data storage. Nature materials. 2007; 6(11): 824–832.
2. Liu, G., Wu, L., Zhu, M., Song, Z., Rao, F., Song, S., Cheng, Y. The investigations of characteristics of Sb2Te as a base phase-change material. Solid-State Electronics. 2017; 135: 31–36.
3. Raoux, S., Wełnic, W., Ielmini, D. Phase change materials and their application to nonvolatile memories. Chemical reviews. 2010; 110(1): 240–267.

4. Kolobov, A. V., Fons, P., Frenkel, A. I., Ankudinov, A. L., Tominaga, J., Uruga, T. Understanding the phase-change mechanism of rewritable optical media. Nature materials. 2004; 3(10): 703–708.
5. Rao, F., Zhang, W., Ma, E. Catching structural transitions in liquids. Science. 2019; 364(6445): 1032–1033.
6. Wang, X. P., Li, X. B., Chen, N. K., Chen, Q. D., Han, X. D., Zhang, S., Sun, H. B. Element-specific amorphization of vacancy-ordered GeSbTe for ternary-state phase change memory. Acta Materialia. 2017; 136: 242–248.
7. Rocca, J., García, J. L., Ureña, M. A., Fontana, M., Arcondo, B. Temperature dependence of electrical resistance in Ge-Sb-Te thin films. Materials Research. 2019; 22(2): 1–7.
8. Siegrist, T., Jost, P., Volker, H., Woda, M., Merkelbach, P., Schlockermann, C., Wuttig, M. Disorder-induced localization in crystalline phase-change materials. Nature materials. 2011; 10(3): 202–208.
9. Poudeu, P. F., Kanatzidis, M. G. Design in solid state chemistry based on phase homologies. Sb 4 Te 3 and Sb 8 Te 9 as new members of the series (Sb 2 Te 3) m·(Sb 2) n. Chemical Communications. 2005; 21: 2672–2674.
10. Kifune, K., Kubota, Y., Matsunaga, T., Yamada, N. Extremely long period-stacking structure in the Sb–Te binary system. Acta Crystallographica Section B: Structural Science. 2005; 61(5): 492–497.
11. Hsu, Y. S., Her, Y. C., Cheng, S. T., Tsai, S. Y. Influence of Al doping on the phase change kinetics of eutectic Sb70Te30 recording film. Optical Data Storage Topical Meeting IEEE. 2006: 85–87.
12. Her, Y. C., Chen, H., Hsu, Y. S. Effects of Ag and In addition on the optical properties and crystallization kinetics of eutectic Sb 70 Te 30 phase-change recording film. Journal of applied physics. 2003; 93(12): 10097–10103.
13. Hsu, Y. S., Her, Y. C., Cheng, S. T., Tsai, S. Y. Thermal-and Laser-Induced Order–Disorder Switching of Ag-Doped Fast-Growth Sb70Te30 Phase-Change Recording Films. Japanese journal of applied physics. 2007; 46(6S): 3945.
14. Prokhorov, E., Mendoza-Galván, A., González-Hernández, J., Chao, B. Effects of Ge addition on the optical and electrical properties of eutectic Sb70Te30 films. Journal of non-crystalline solids. 2007; 353(18–21): 1870–1874.
15. Her, Y. C., Hsu, Y. S. Optical properties and crystallization characteristics of Ge-doped Sb70Te30 phase change recording film. Japanese journal of applied physics. 2003; 42(2S): 804.
16. Hsu, Y. S., Her, Y. C., Cheng, S. T., Tsai, S. Y. (2007). Thermal and Laser Induced Order Disorder Switching of In Doped Fast Growth Sb70Te30 Phase Change Recording Films. IEEE transactions on magnetics. 2007; 43(2): 936–938.
17. Wang, G., Li, J., Qi, D., Nie, Q., Shen, X., Lu, Y. Controllable phase separation and improved grain growth mode of Mg-doped Sb7Te3 films. Ceramics International. 2017; 43(15): 12452–12458.
18. Hsu, Y. S., Liu, Y. D., Her, Y. C., Cheng, S. T., Tsai, S. Y. (2009). Crystallization and Melting Kinetics of Zn-Doped Fast-Growth Sb70Te30 Phase-Change Recording Films. Japanese Journal of Applied Physics. 2009; 48(3S1): 03A061.

19. Wang, G., Shen, X., Nie, Q., Wang, R. P., Wu, L., Lu, Y., Chen, Y. Improved phase-change characteristics of Zn-doped amorphous Sb7Te3 films for high-speed and low-power phase change memory. Applied Physics Letters. 2013; 103(3): 031914.
20. Lin, C., Hu, J., Wei, T., Li, W., Ling, Y., Liu, Q., Liu, B. Excellent thermal stability attributed to Cr dopant in Sb2Te phase change material. Materials Letters. 2022; 315: 131977.
21. Zhao, Z. Y., Peng, S., Tan, Z. L., Wang, C. J., Wen, M. Doping effects of Ru on Sb2Te and Sb2Te3 as phase change materials studied by first-principles calculations. Materials Today Communications. 2022; 31: 103669.
22. Lu, Y., Song, S., Song, Z., Rao, F., Wu, L., Zhu, M., Yao, D. Investigation of CuSb4Te2 alloy for high-speed phase change random access memory applications. Applied Physics Letters. 2012; 100(19): 193114.
23. Gu, Y., Song, S., Song, Z., Cheng, Y., Du, X., Liu, B., Feng, S. SixSb2Te materials with stable phase for phase change random access memory applications. Journal of Applied Physics. 2012; 111(5): 054319.
24. Zheng, Y., Cheng, Y., Zhu, M., Ji, X., Wang, Q., Song, S., Feng, S. A candidate Zr-doped Sb2Te alloy for phase change memory application. Applied Physics Letters. 2016; 108(5): 052107.
25. Zhu, M., Wu, L., Song, Z., Rao, F., Cai, D., Peng, C., Feng, S. Ti10Sb60Te30 for phase change memory with high-temperature data retention and rapid crystallization speed. Applied Physics Letters. 2012; 100(12): 122101.
26. Peng, C., Wu, L., Rao, F., Song, Z., Yang, P., Song, H., Chu, J. W-Sb-Te phase-change material: A candidate for the trade-off between programming speed and data retention. Applied Physics Letters. 2012; 101(12):122108.
27. Rocca, J. A., Bilovol, V., Errandonea, D., Rebaza, A. G., Navarro, A. M., Chanduví, H. M., Ureña, M. A. (2019). Structural and Mössbauer study of (Sb0. 70Te0. 30) 100-x Snx alloys with x = 0, 2.5, 5.0 and 7.5. Journal of Alloys and Compounds. 2019; 795: 27–33.
28. Erazú, M., Rocca, J., Fontana, M., Ureña, A., Arcondo, B., Pradel, A. Raman spectroscopy of chalcogenide thin films prepared by PLD. Journal of Alloys and Compounds. 2010; 495(2): 642–645.
29. Bilovol, V., Fontana, M., Rocca, J. A., Chanduvi, H. M., Navarro, A. M., Rebaza, A. G., Ureña, A. M. Structural, vibrational and electronic properties in the glass-crystal transition of thin films Sb70Te30 doped with Sn. Journal of Alloys and Compounds. 2020; 845: 156307.
30. Waseda Y. The Structure of Non-Crystalline Materials. McGraw Hill Inc. USA. 1980.
31. Her, Y. C., Hsu, Y. S. Thickness dependence of crystallization and melting kinetics of eutectic Sb70Te30 phase change recording film. Journal of non-crystalline solids. 2008; 354(27): 3129–3134.
32. Prokhorov, E., Mendoza-Galván, A., González-Hernández, J., Chao, B. Effects of Ge addition on the optical and electrical properties of eutectic Sb70Te30 films. Journal of non-crystalline solids. 2007; 353(18–21): 1870–1874.

33. Prokhorov, E., González-Hernández, J., Mendoza-Galván, A., Trapaga, G., Luna-Bárcenas, G. Structural and electrical properties of Germanium-doped Sb70Te30 eutectic thin films. Journal of non-crystalline solids. 2011; 357(7); 1610–1614.
34. Cheng, H. Y., Kao, K. F., Lee, C. M., Chin, T. S. Characteristics of Ga–Sb–Te films for phase-change memory. IEEE transactions on magnetics. 2007; 43(2): 927–929.
35. Kao, K. F., Cheng, H. Y., Jong, C. A., Lan, C. J., Chin, T. S. Tungsten Added Sb80 Te20 for Phase-Change RAM. IEEE transactions on magnetics. 2007; 43(2): 930–932.
36. Raoux, S., Salinga, M., Jordan-Sweet, J. L., Kellock, A. Effect of Al and Cu doping on the crystallization properties of the phase change materials SbTe and GeSb. Journal of Applied Physics. 2007; 101(4): 044909.
37. Kissinger, H. E. Reaction kinetics in differential thermal analysis. Analytical chemistry. 1957; 29(11): 1702–1706.
38. Fontana, M., Arcondo, B., Clavaguera-Mora, M. T., Clavaguera, N. Crystallization kinetics driven by two simultaneous modes of crystal growth. Philosophical Magazine B. 2000; 80(10): 1833–1856.
39. Clavaguera, N., Clavaguera-Mora, M. T., Fontana, M. Accuracy in the experimental calorimetric study of the crystallization kinetics and predictive transformation diagrams: Application to a Ga–Te amorphous alloy. Journal of Materials research. 1998; 13(3): 744–753.
40. Tao, W., Li, K., Hu, J., Liu, Q., Cheng, M., Li, W.,Liu, B. High optical/color contrast of Sb2Te thin film and its structural origin. Materials Science in Semiconductor Processing. 2022; 144: 106619.
41. Zhou, G. F. Materials aspects in phase change optical recording. Materials Science and Engineering: A. 2011; 304: 73–80.
42. Ahmed, S., Wang, X., Li, H., Zhou, Y., Chen, Y., Sun, L., Mazzarello, R. Change in Structure of Amorphous Sb–Te Phase-Change Materials as a Function of Stoichiometry. Physica status solidi (RRL)–Rapid Research Letters. 2021; 15(6): 2100064.
43. Rocca, J. A., Ureña, M. A., Fontana, M. R. Curva maestra para la cristalización de aleaciones amorfas Sb70Te30. Anales Asociación Física Argentina. 2023; 34(1): 22–26.
44. Clavaguera-Mora, M. T. Glassy materials: thermodynamic and kinetic quantities. Journal of alloys and compounds. 1995; 220(1–2): 197–205.
45. Diego, J. A., Clavaguera-Mora, M. T., Clavaguera, N. Thermodynamic, kinetic and structural mechanisms controlling the formation of nanocrystalline NdFeB materials. Materials Science and Engineering A. 1994; 179: 526–530.
46. Clavaguera-Mora, M. T., Clavaguera, N., Crespo, D., Pradell, T. Crystallisation kinetics and microstructure development in metallic systems. Progress in Materials Science. 2002; 47(6): 559–619.
47. Fontana, M., Arcondo, B., Clavaguera-Mora, M. T., Clavaguera, N., Greneche, J. M. Crystallization kinetics and structural aspects of TeGaSn amorphous alloys. Journal of Applied Physics. 2000; 88(6): 3276–3284.

48. Fontana, M., Arcondo, B., Clavaguera-Mora, M. T., Clavaguera, N. Crystallization kinetics driven by two simultaneous modes of crystal growth. Philosophical Magazine B. 2000; 80(10): 1833–1856.
49. Turnbull, D. Formation of crystal nuclei in liquid metals. Journal of Applied Physics. 1950; 21(10): 1022–1028.
50. J.H. Perepezco,in: R. Mehrabian,B.H. Kear,M. Cohen (Eds.),Rapid Solidificaion Processing Principles and Technologies, Claitor's, Baton Rouge, LA, 1980: 56.
51. Urena, A., Fontana, M., Arcondo, B., Clavaguera-Mora, M. T.,Clavaguera, N. Influence of Cu addition in the crystallization of the superionic glass (Ge25Se75) 75Ag25. Journal of non-crystalline solids. 2002; 304(1–3): 306–314.
52. Fontana, M., Arcondo, B., Clavaguera-Mora, M. T., Clavaguera, N. Mechanisms controlling primary crystallisation of Ga20Te80 glasses. Journal of non-crystalline solids 2007; 353(22–23): 2131–2142.
53. Chebli, K., Saiter, J. M., Grenet, J., Hamou, A., Saffarini, G. Strong-fragile glass forming liquid concept applied to GeTe chalcogenide glasses. Physica B: Condensed Matter. 2001; 304(1–4): 228–236.
54. Wei, S. Anomalous liquids on a new landscape: From water to phase-change materials. Journal of Non-Crystalline Solids. 2002; X, 14, 100094.
55. Wei, S., Coleman, G. J., Lucas, P., Angell, C. A. Glass transitions, semiconductor-metal transitions, and fragilities in Ge – V– Te (V = As, Sb) liquid alloys: The difference one element can make. Physical Review Applied. 2017; 7(3): 034035.
56. Lankhorst, M. H. R. Modelling glass transition temperatures of chalcogenide glasses. Applied to phase-change optical recording materials. Journal of non-crystalline solids. 2002; 297(2–3): 210–219.
57. Kang, L., Chen, L.. First-principles study of the liquid and amorphous phases of Sb2Te phase change memory material. Journal of Physics: Condensed Matter. 2021; 33(16): 165703.
58. Luo, Y. R., & Kerr, J. A. Bond dissociation energies. CRC handbook of chemistry and physics. 2012; 89.

Tables

Table 1: Name of the studied samples

Composition (at. %)	Name
$Sb_{70}Te_{30}$	$Sb_{70}Te_{30}$
$Ag_{7.5}(Sb_{0.70}Te_{0.30})_{92.5}$	AST7.5
$Sn_{7.5}(Sb_{0.70}Te_{0.30})_{92.5}$	SST7.5

Table 2: Thermal magnitudes of the studied samples: The peak temperature of the crystallization T_p, the onset temperature T_{on} (measured to β = 20 K/min), the melting temperature T_m, the crystallization enthalpy ΔH_c, the melting enthalpy ΔH_m, the activation energy E_a , for the different peaks of crystallization of the samples $Sb_{70}Te_{30}$, AST7.5 and SST7.5 .

$Sb_{70}Te_{30}$		
T_m (K)	813	
ΔH_m (J/g)	138	
First crystallization peak		
T_{on} (K)	400	
E_a (kJ/mol)	190 ± 10	
β (K/min)	T_p (K)	ΔH_c (J/g)
10	413.3	17.1
20	419.7	17.8
40	424.5	17.8
80	428.6	19.1

AST7.5		
T_m (K)	788	
ΔH_m (J/g)	130	
First crystallization peak		
T_{on} (K)	436	
E_a (kJ/mol)	210 ± 10	
β (K/min)	T_p (K)	ΔH_c (J/g)
10	435.9	7.6
20	440.0	7.5
40	445.5	7.7
80	451.4	12.2
Second crystallization peak		
E_a (kJ/mol)	190 ± 30	
Third crystallization peak		
E_a (kJ/mol)	140 ± 40	
ΔH_c (J/g)	17	

SST7.5		
T_m (K)	819	
ΔH_m (J/g)	146	
First crystallization peak		
T_{on} (K)	410	
E_a (kJ/mol)	310 ± 10	
β (K/min)	T_p (K)	ΔH_c (J/g)
10	427.6	14.8
20	430.6	13.9
40	434.3	16.4
80	437.9	15.2
Second crystallization peak		
ΔH_c (J/g)	15	

Table 3: Measured, estimated and fitted values used to model the first crystallization steps of the samples $Sb_{70}Te_{30}$, AST7.5 and SST7.5.

Sample	$Sb_{70}Te_{30}$	AST7.5	SST7.5
	Measured Parameters:		
ΔH_m (kJ/mol)	17.044	15.903	17.980
T_m (K)	813	788	819
	Estimated Parameters:		
Γ	0.9	0.9	0.9
a_o (m)	$1.6\ 10^{-10}$	$1.6\ 10^{-10}$	$1.6\ 10^{-10}$
L^2/λ	1.0	1.0	1.0
$\eta(T_m)$(Pa s)	0.005	0.005	0.005
	Fitted Parameters:		
N_v/L^2 ($1/cm^3$) ± 10 %	$3\ 10^9$	$2\ 10^{10}$	$2\ 10^{15}$
A (K) ± 5 %	640	891	1010
T_o (K) ± 4	339	356	349

Figures

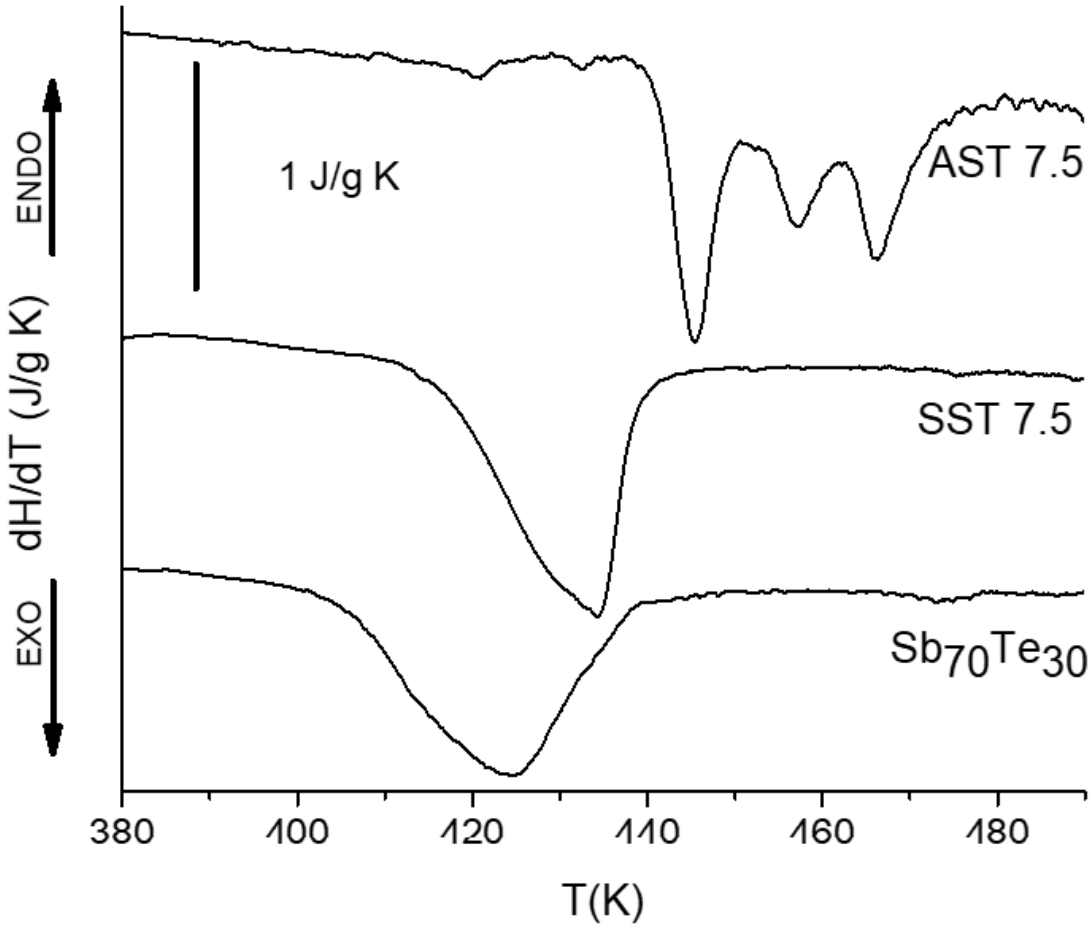

Figure 1

Calorimetric signal (normalized by the mass and the heating rate) *dH/dT* of the $Sb_{70}Te_{30}$, AST7.5 and SST7.5 samples obtained under a continuous heating regime with β = 40 K/min.

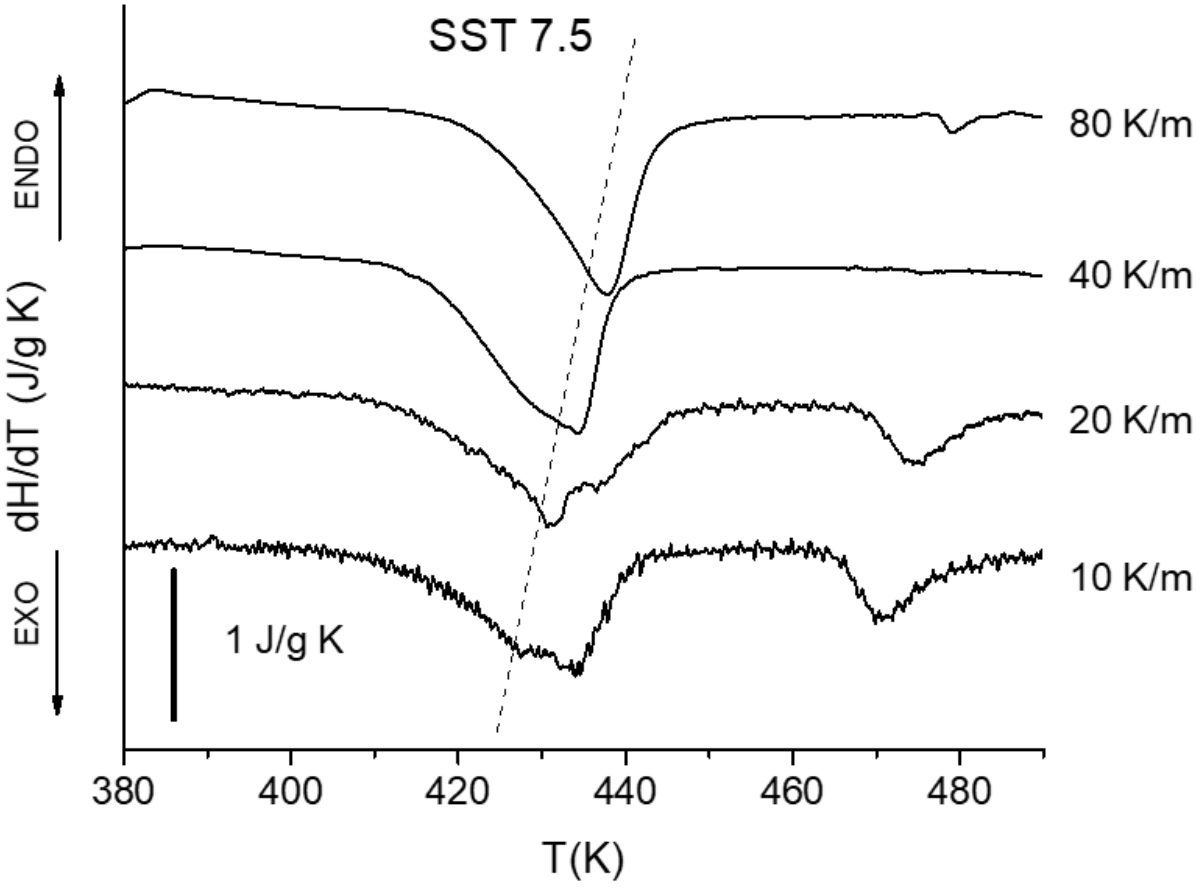

Figure 2

Calorimetric signal (normalized by the mass and the heating rate) *dH/dT* of the SST7.5 sample obtained under a continuous heating regime with β = 10, 20, 40 and 80 K/min.

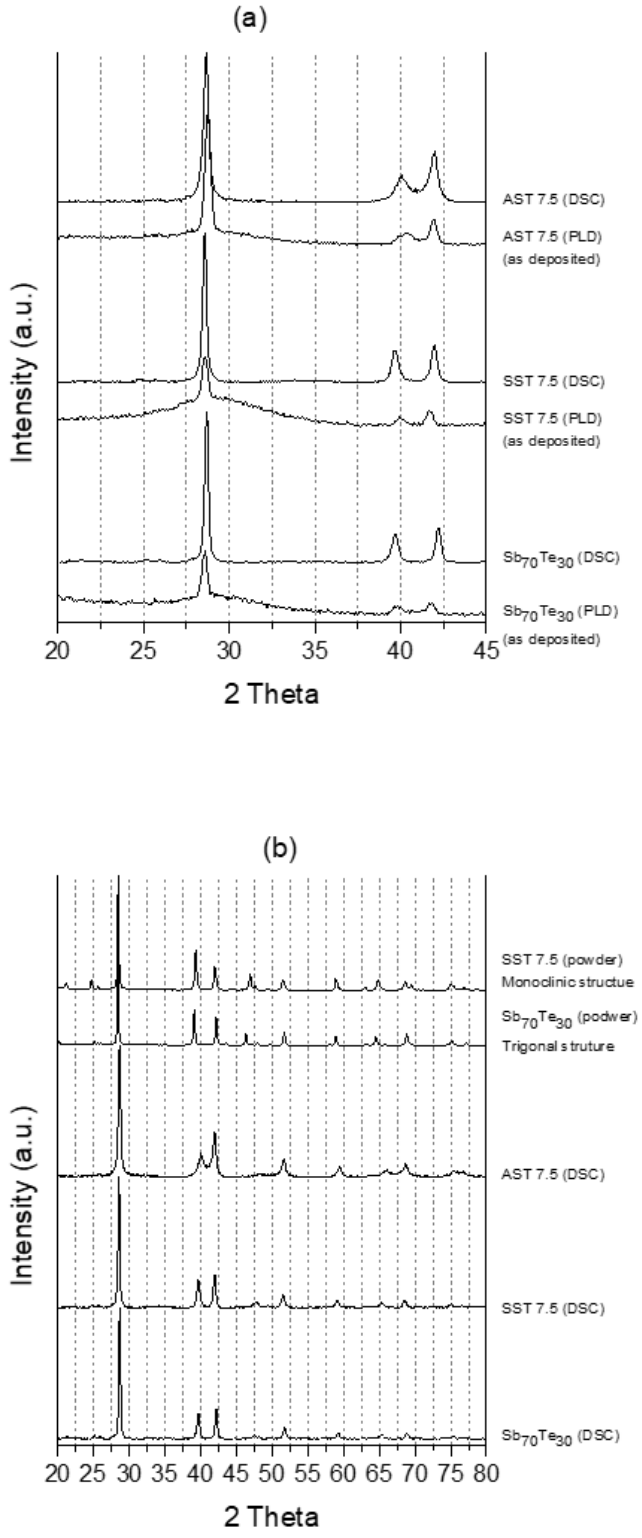

Figure 3

X Ray Diffraction patterns of the studied samples (a) thin films as deposited and after DSC experiments at 2θ range 20-45°, (b) thin films after DSC experiments at 2 θ range 20-80°, and, as-cast sample powder of compositions $Sb_{70}Te_{30}$ and SST7.5.

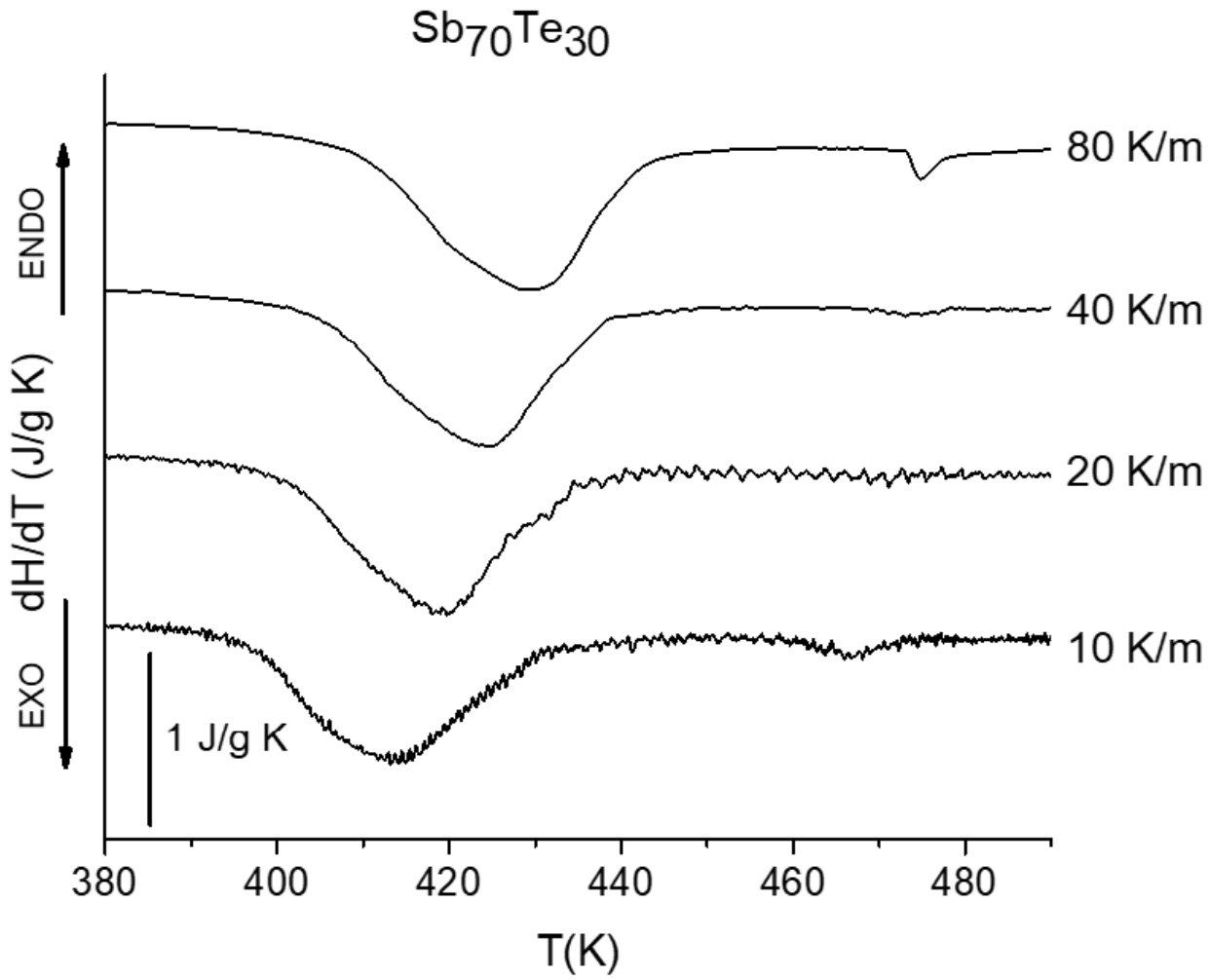

Figure 4

Calorimetric signal (normalized by the mass and the heating rate) *dH/dT* of the $Sb_{70}Te_{30}$ sample obtained under a continuous heating regime with β = 10, 20, 40 and 80 K/min.

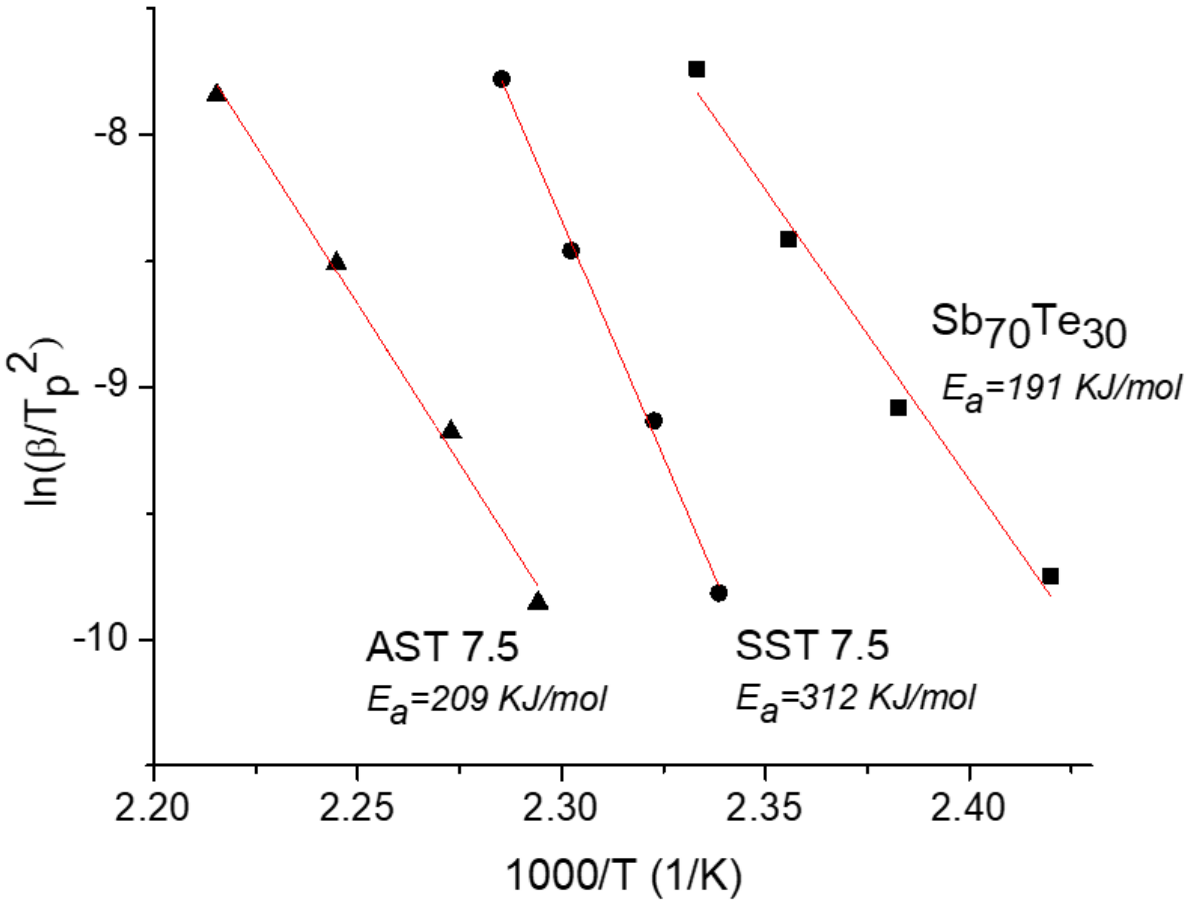

Figure 5

Kissinger method. $\ln(\beta/(T_p^2))$ versus $1000/T_p$ obtained for the crystallization of $Sb_{70}Te_{30}$, AST7.5 and SST7.5 thin films.

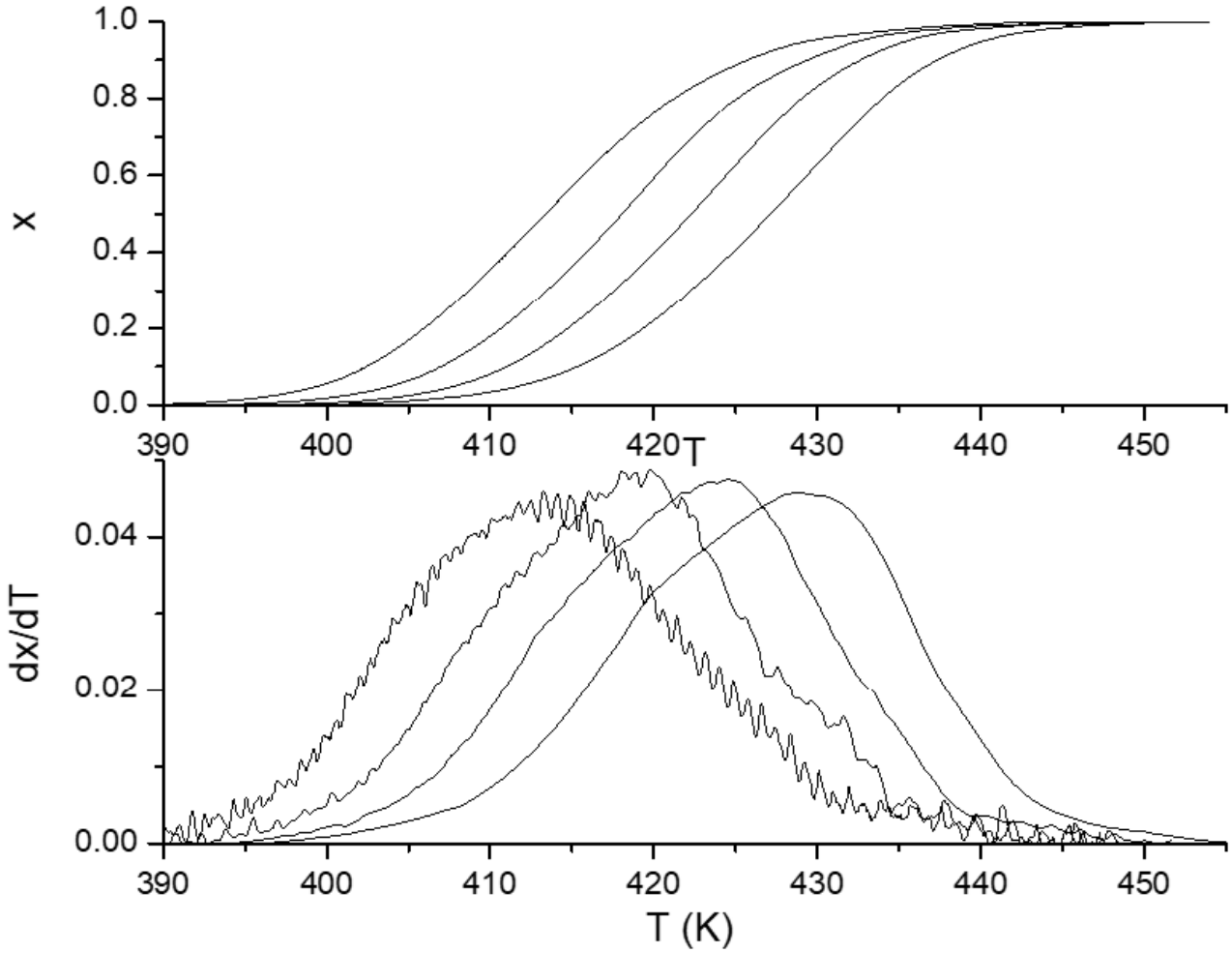

Figure 6

Transformed fraction *x* and transformation rate *dx/dt* normalized by the heating rate (*dx/dT*) obtained for the crystallization of the $Sb_{70}Te_{30}$ thin film.

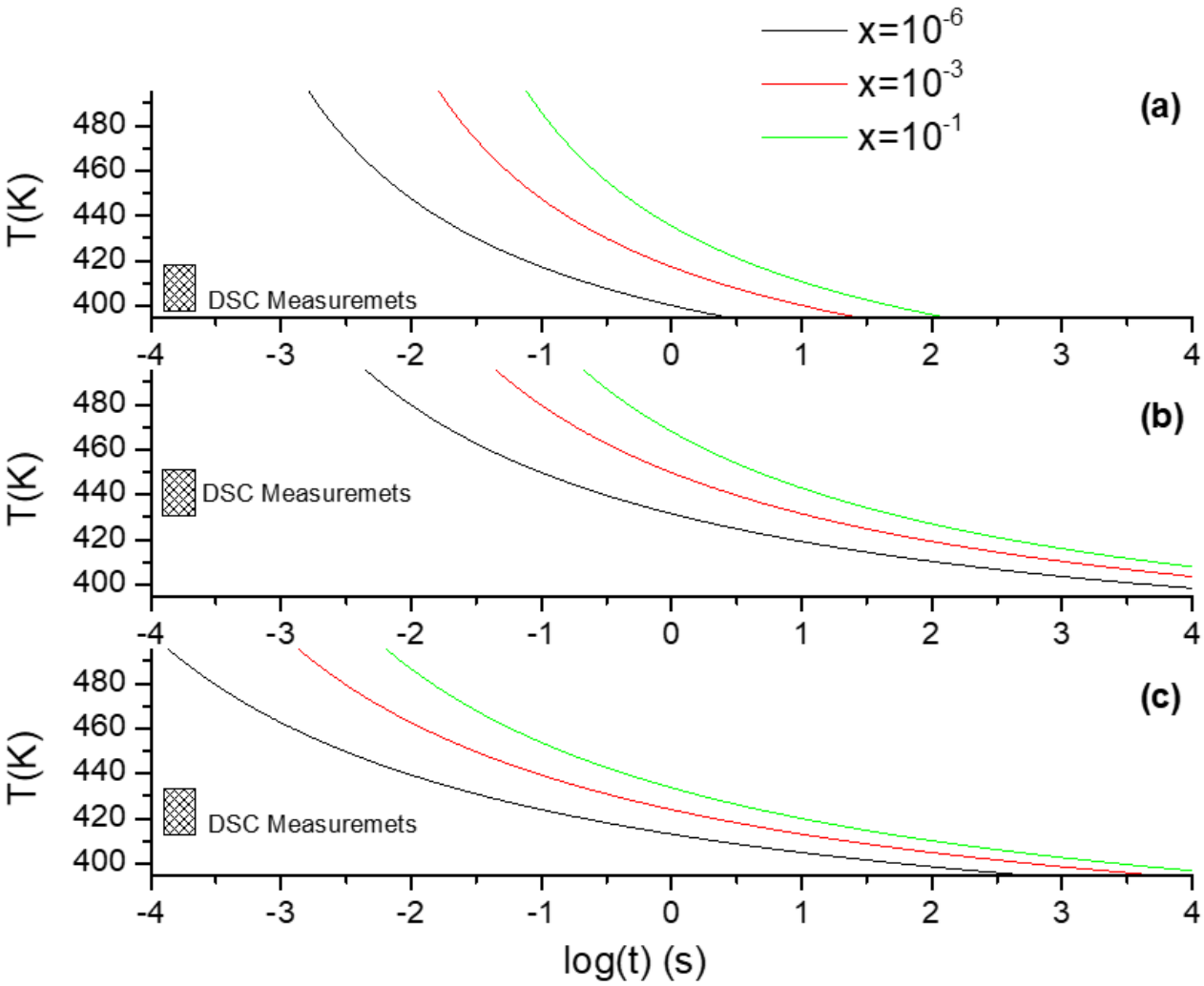

Figure 7

Time temperature transformation (TTT) curves for different crystallized fractions (x = 10^{-6}, 10^{-3} and 0.1) obtained for the crystallization of $Sb_{70}Te_{30}$, AST7.5 and SST7.5 samples. The temperature range of the DSC measurements is shown.

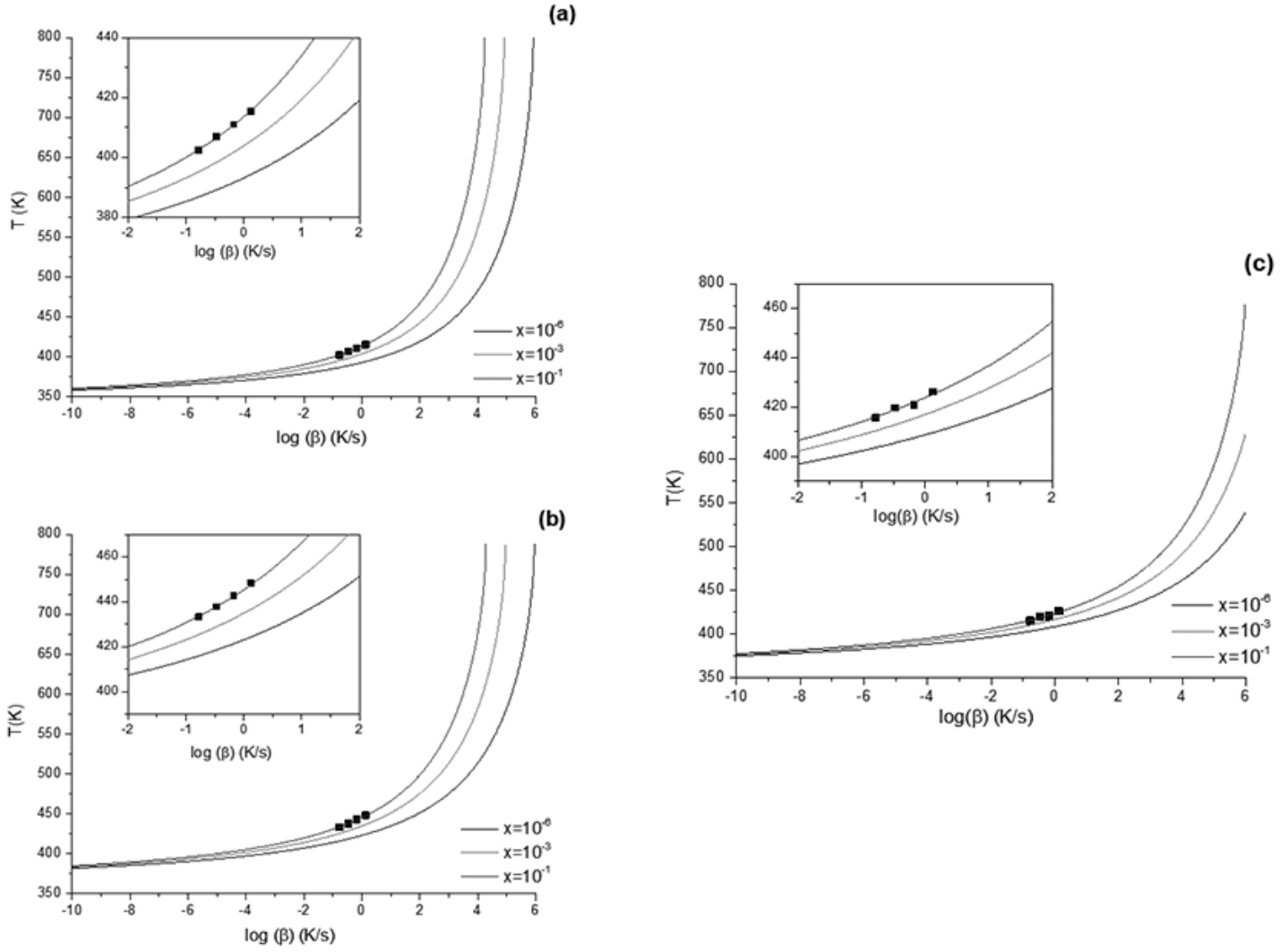

Figure 8

Calculated temperature-heating rate (THrT) curves for different crystallized fractions (x = 10^{-6}, 10^{-3} and 0.1) obtained for the crystallization of (a) $Sb_{70}Te_{30}$, (b) AST7.5 and (c) SST7.5 samples. Experimental data for x = 0.1 obtained using DSC are shown with square symbols. A detail of the agreement between the experimental data and the calculated curve is shown in the inset figure.

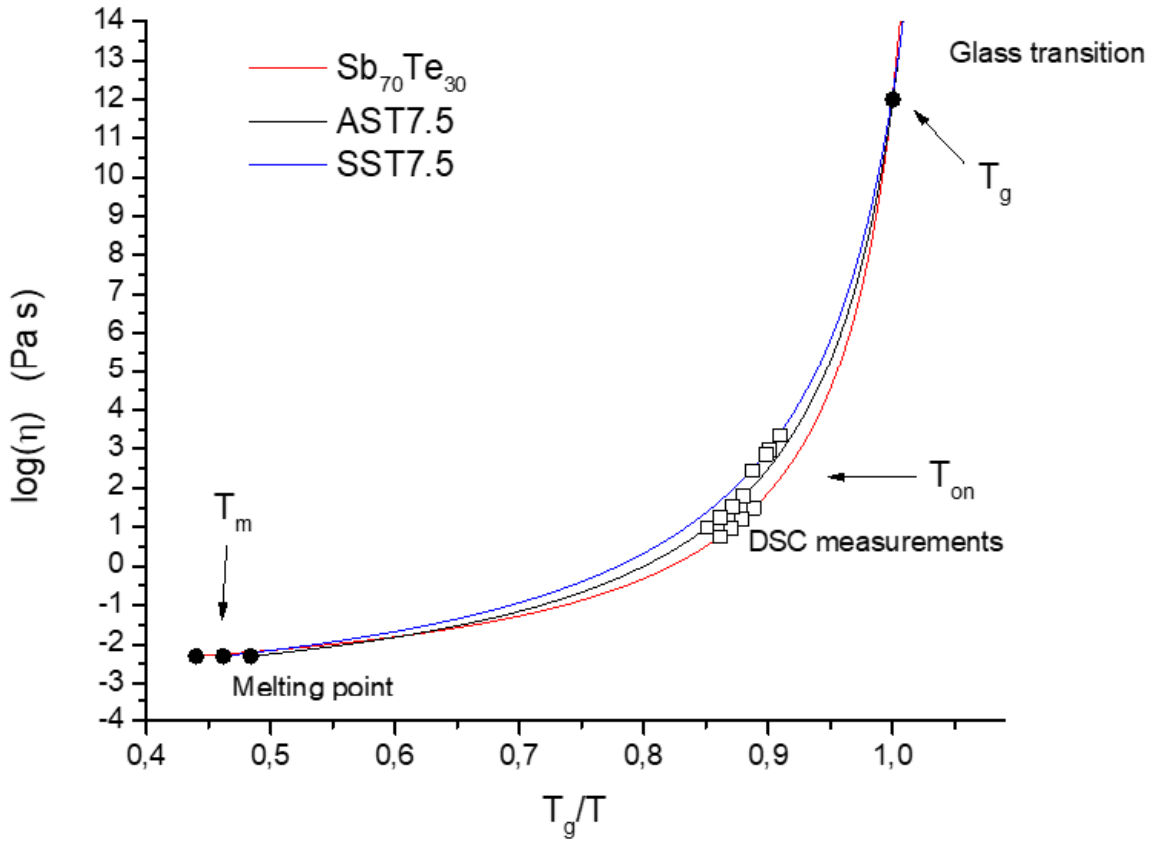

Figure 9

Temperature dependence of the viscosity for $Sb_{70}Te_{30}$, AST7.5 and SST7.5 samples obtained using Eq (4) and Table 3. The three temperature zones, where the experimental or reference data are known (glass transition, DSC data and melting point) are shown.